

Anomalous Refraction of Spin Waves as a Way to Guide Signals in Curved Magnonic Multimode Waveguides


Szymon Mieszczak^{1,*}, Oksana Busel^{2,†}, Paweł Gruszecki^{1,3}, Andriy N. Kuchko^{2,4},
Jarosław W. Kłos¹ and Maciej Krawczyk¹

¹*Faculty of Physics, Adam Mickiewicz University, Poznań, Uniwersytetu Poznańskiego 2, Poznań 61-614, Poland*

²*National Technical University of Ukraine “Igor Sikorsky Kyiv Polytechnic Institute”, Peremohy Ave. 37, Kyiv 03056, Ukraine*

³*Institute of Molecular Physics, Polish Academy of Sciences, Mariana Smoluchowskiego 17, 60-179 Poznań, Poland*

⁴*Institute of Magnetism of NAS of Ukraine, Vernadskogo Ave. 36b, Kyiv 03142, Ukraine*

 (Received 31 January 2020; revised 6 April 2020; accepted 22 April 2020; published 15 May 2020; corrected 15 October 2020)

We present a method for efficient spin-wave guiding within the magnonic nanostructures. Our technique is based on the anomalous refraction in the metamaterial flat slab. The gradual change of the material parameters (saturation magnetization or magnetic anisotropy) across the slab allows tilting the wavefronts of the transmitted spin waves and controlling the refraction. Numerical studies of the spin-wave refraction are preceded by the analytical calculations of the phase shift acquired by the spin wave due to the change of material parameters in a confined area. We demonstrate that our findings can be used to guide the spin waves smoothly in curved waveguides, even through sharp bends, without reflection and scattering between different waveguide's modes, preserving the phase, the quantity essential for wave computing.

DOI: [10.1103/PhysRevApplied.13.054038](https://doi.org/10.1103/PhysRevApplied.13.054038)

I. INTRODUCTION

Phase and amplitude are the fundamental characteristics of waves. The processing of any kind of wave relies on the interference effects, which depend on these characteristics. Thus, the control of spin waves' (SWs') phase and amplitude is essential in magnonics [1] to perform both analog [2,3] and digital [4] SW-based computing [5].

One of the significant challenges limiting the application of SWs relates to the capability of coherent and weakly damped signal transmission. Fulfilling this condition is necessary to transmit the information, encoded in SW phase or amplitude, between particular parts of a magnonic circuit, sometimes in a grid of interconnected and crossed waveguides, enabling a flow of SWs in different directions [4,6]. Typically, the interconnections are realized by waveguides being narrow and flat ferromagnetic stripes. Here arises the problem of the SW scattering on bends of waveguides. If the static magnetization is saturated and oriented along the direction of the external magnetic field [7], then the (static and dynamic) magnetic surface charges, generated by the normal to the surface component of the magnetization, changes at the bends of the waveguide. On the

other hand, if the external magnetic field is low [8] or the waveguide is properly patterned [9], the static magnetization follows the shape of the curved waveguide due to the shape anisotropy, which minimizes the changes of magnetic charges at bends. Nevertheless, the magnetic volume charges are generated due to curvilinear magnetic configuration in this system. In addition, the exchange interaction is modified, which induces the effects equivalent to the presence of the anisotropy field or the field of Dzyaloshinskii-Moriya interaction [10–12].

The SWs' wavelength is a few orders of magnitude shorter than the electromagnetic waves of corresponding frequencies [2]. Therefore, typical magnonic waveguides of the width accessible in photolithographic fabrication techniques are multimodal waveguides even in the GHz-frequency range. The fabrication of a single-mode waveguide for SWs is difficult since their widths need to be narrow, especially for high-frequency SWs [13]. Also, the generation of high-frequency harmonic SWs is challenging and requires the modification of the standard methods, based on the SW excitation by radiofrequency field. The different approaches use the effects of SW confinement, interference in periodic gratings, coupling between the materials of high and low ferromagnetic resonance frequency or spin vortex core [14–17]. The phase-sensitive mapping of SW profiles can be achieved using the

*szymon.mieszczak@amu.edu.pl

†opbusel@gmail.com

micro-Brillouin light scattering [18,19], which is however limited in resolution to 200 nm. Only with a sophisticated extension, is it possible to detect SWs with Brillouin light scattering with a resolution below 100 nm [20]. The finer resolution can be gained using x-ray microscopy [21] where the x-ray magnetic circular dichroism is used to find the spatial map of the phase [22].

To date, the single-mode waveguides for short SWs can be realized in the systems utilizing domain walls as magnonic waveguides since they can create narrow potential wells where SW modes can be localized and propagate lengthwise [23–29]. Difficulties associated with SW wavelengths' dependence on the direction of propagation (anisotropic dispersion relation) are negligible for short-wavelength SWs where exchange interactions of isotropic nature dominate over the anisotropic dipolar interactions. Also, for the magnetic configuration where the magnetic field is applied perpendicularly to the film's surface, the SW dynamics is naturally isotropic, independently on the frequency of SW. The only obstacle related to that geometry is a high bias field demanded to magnetize the sample uniformly. It can be overcome in materials with strong out-of-plane anisotropy, but these are usually characterized by high SW damping.

In multimode waveguides, the mechanism, which leads to the decoherence of the propagating SWs is scattering to other, perpendicularly quantized modes. Therefore, the signal loses the information encoded in the phase. Another consequence is that the SW propagates along a longer zig-zag-shaped path [30], which can also be interpreted as a redistribution of the momentum (wave vector) between the components, that are transferal and longitudinal to the waveguide's axis. It is worthwhile to note, that the transverse quantization of the modes in the planar waveguide is related not only to the width of the structure but can also be introduced additionally by the periodic patterning along the waveguide [31–34].

We point out that the scattering between the modes is one of the most important factors for the SW decoherence at the bends of the magnonic waveguide. Therefore, the question arises: can we modify the properties of the bending region to block the redistribution of incoming mode into the different outgoing modes, keeping the transmission as high as possible? One possible solution is to fill the bending region by the material of spatially tailored properties, which refract the SW and redirect its propagation strictly along the outgoing section of the waveguide. In other words, we should look for the particular kind of so-called graded index (GRIN) element for SWs [35–43]. Recently GRIN elements have been used to bend SWs for in-plane [37] and out-of-plane [40] magnetized films. Another exciting idea is an application of SW lenses, in particular flat metalenses [44], i.e., lenses of fixed width introducing different phase delay of transmitted waves alongside the interface. Except for the changes

in the phases of refracted waves, the GRIN element should not introduce significant changes to their amplitudes. The interplay between the material parameters of the slab and its sizes determines the conditions for the resonant transmission [45,46]. Therefore, we need to design a system to work in the conditions close to the resonant transmission.

In this paper, we employ the anomalous refraction [47] achieved in the GRIN slab to change the direction of coherently propagating SWs at the bend of the waveguide. For anomalous refraction, the wavefronts of refracted waves are tilted at a desirable angle with respect to wavefronts of the incident waves, even at normal incidence. This phenomenon requires a linear change of the phase of the transmitted waves alongside the interface, where the refraction takes place. Its description requires the generalization of Snell's law [47,48]. We develop the analytical theory for the scattering of exchange SWs on the homogeneous ferromagnetic slab of finite width embedded in a ferromagnetic layer. Minimizing the total energy, we derive the boundary conditions on the interfaces between the slab and its surroundings. We obtain the complete relations between the phases and amplitudes of the incident and scattered SWs. These calculations are successfully compared to micromagnetic simulations. Then, we use our findings to demonstrate both analytically and numerically an anomalous refraction for the purely exchange SWs incident from a waveguide to a semi-infinite film through a flat magnonic GRIN slab. We treat the GRIN element as an inhomogeneous slab linking the input and output branches of the waveguide at the bend.

The paper is organized as follows. In the next section, we describe the analytical model. In Sec. III we show and discuss the results of the analytical and numerical studies, which are summarized in Sec. IV. In Appendix A we present details of analytical calculation, while in Appendix B details of micromagnetic simulations.

II. MODEL AND METHODS

A. Boundary-condition problem

Let us consider SWs propagating (along the x axis) through a ferromagnetic layer B ($0 < x < d$) embedded as a slab between two half-spaces of the ferromagnetic matrix A ($x \leq 0$ and $x \geq d$), as shown in Fig. 1. The slab B is exchange coupled by thin interfaces of thickness δ to the matrix A . For simplicity's sake, we assume that the system is uniform and infinitely extended in the x - z plane. We consider the case when the static magnetizations \mathbf{M}_A and \mathbf{M}_B are oriented along the z axis (see Fig. 1) and are parallel to each other everywhere in the system: $\mathbf{M}_{A(B)} = [0, 0, M_{S,A(B)}]$, where $M_{S,A(B)}$ denotes the saturation magnetization. The indexes A and B denote materials of the matrix and the slab, respectively.

The dynamics of magnetization in an effective magnetic field can be described by the Landau-Lifshitz equation

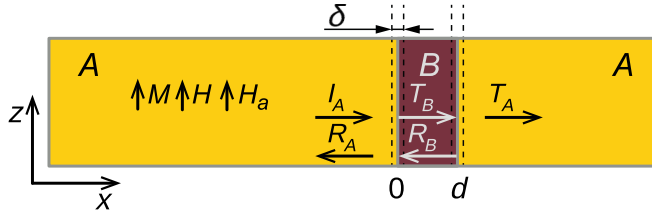


FIG. 1. Scattering of the SWs on a ferromagnetic layer (dark area) embedded in a ferromagnetic matrix (light area). The uniaxial anisotropy field H_a and the static magnetization M for ferromagnetic matrix (A) and layer (B) are parallel to each other and tangential to the plane of the layer. The layer B of thickness d is exchange coupled to the matrix A by the interfaces of thickness δ .

(LLE):

$$\frac{\partial \mathbf{M}_{A(B)}}{\partial t} = -\mu_0 |\gamma| [\mathbf{M}_{A(B)} \times \mathbf{H}_{\text{eff},A(B)}], \quad (1)$$

where the effective field is a variational derivative of the energy W with respect to the magnetization vector: $\mathbf{H}_{\text{eff},A(B)} = -(1/\mu_0)\delta W/\delta \mathbf{M}_{A(B)}$. The parameter γ is the gyromagnetic ratio and μ_0 is the permeability of the vacuum. The total magnetic energy density of the system w includes the following: the density of the Zeeman energy $(-\mu_0 \mathbf{H} \cdot \mathbf{M}_{A(B)})$, with the external magnetic field \mathbf{H} ; the exchange energy density $[1/2\alpha_{A(B)}(\partial \mathbf{M}_{A(B)}/\partial x_i)^2]$, with the exchange interaction parameter $\alpha_{A(B)} = 2A_{\text{ex},A(B)}/M_{S,A(B)}^2$, where $A_{\text{ex},A(B)}$ is the exchange stiffness constant in the material A or B , respectively; the density of anisotropy energy $[-1/2\beta_{A(B)}(\mathbf{M}_{A(B)} \cdot \mathbf{n}_a)^2]$, where $\beta_{A(B)} = 2K_{A(B)}/M_{S,A(B)}^2$ and \mathbf{n}_a is the unit vector of the easy axis. Anisotropy energy density is expressed by the uniaxial anisotropy constant $K_{A(B)}$. Assuming that the thickness of the interface δ is smaller than the exchange length $\lambda_{\text{ex}} = \sqrt{2A_{\text{ex}}/\mu_0 M_S^2}$, we can neglect the structure of the interfaces (roughness, material mixing) and introduce the coupling parameter A , which is the parameter of the interlayer exchange and can be expressed via the interface thickness δ [49,50]. We postulate the exchange type of coupling characterized by the energy density at the interfaces: $x = 0, d$ (i.e., the energy per unit area): $-A \mathbf{M}_A \cdot \mathbf{M}_B$, where $A = (A_{\text{ex},A} + A_{\text{ex},B})/(2M_{S,A}M_{S,B}\delta)$ is coupling parameter.

Minimizing the total energy, we can derive boundary conditions:

$$\begin{cases} \left(\alpha_A \frac{\partial}{\partial x} + A \frac{M_{S,B}}{M_{S,A}} \right) m_A - A m_B = 0 \\ \left(\alpha_B \frac{\partial}{\partial x} - A \frac{M_{S,A}}{M_{S,B}} \right) m_B + A m_A = 0 \end{cases}, \quad x = 0, \quad (2)$$

$$\begin{cases} \left(\alpha_B \frac{\partial}{\partial x} + A \frac{M_{S,A}}{M_{S,B}} \right) m_B - A m_A = 0 \\ \left(\alpha_A \frac{\partial}{\partial x} - A \frac{M_{S,B}}{M_{S,A}} \right) m_A + A m_B = 0 \end{cases}, \quad x = d. \quad (3)$$

At each interface between matrix and slab, the solutions of the LLE satisfy the boundary conditions for the amplitudes of the dynamical components of magnetization $\mathbf{m}_{A(B)} = [m_{A(B),x}, m_{A(B),y}, 0]$ [for convenience, in Eqs. (2) and (3) they are expressed via the cyclic variables $m_{A(B)} = m_{A(B),x} \pm i m_{A(B),y}$, where i is the imaginary unit] for every interface, namely at $x = 0$ and $x = d$.

We are looking for a solution in linear regime, i.e., describing the harmonic precession with the angular frequency ω : $\mathbf{m}(\mathbf{r}, t) = \mathbf{m}(\mathbf{r}) \exp(i\omega t)$.

For the general stationary solution $\mathbf{m}(\mathbf{r})$, we have to include the waves propagating both to the left and to the right. This can be mathematically expressed as

$$m_A = I_A e^{ik_A x} + r_A e^{-ik_A x}, \quad x \leq 0, \quad (4)$$

$$m_B = t_B e^{ik_B x} + r_B e^{-ik_B x}, \quad 0 < x < d, \quad (5)$$

$$m_A = t_A e^{ik_A x}, \quad x \geq d. \quad (6)$$

The parameters k_A and k_B stand for the wave numbers in the matrix and the slab, respectively. The wave numbers k_A and k_B depend on the external magnetic field H and material parameters: saturation magnetization $M_{S,A(B)}$ and anisotropy field $H_{a,A(B)} = 2K_{A(B)}/(\mu_0 M_{S,A(B)})$. The amplitude of incoming wave is normalized to 1: $I_A = 1$. All the remaining amplitudes r_A, t_B, r_B, t_A are, in general, complex valued: $R_A e^{i\varphi_{R_A}}, T_A e^{i\varphi_{T_A}}, T_B e^{i\varphi_{T_B}}, R_B e^{i\varphi_{R_B}}$ and contain the information about the real amplitudes R_A, T_B, R_B, T_A and phases $\varphi_{R_A}, \varphi_{T_A}, \varphi_{T_B}, \varphi_{R_B}$.

For calculating the complex amplitudes of SWs, namely r_A, t_B, r_B , and t_A [presented in Appendix A, Eqs. (A1)–(A4)], we use the boundary conditions Eqs. (2) and (3).

B. Huygens-Fresnel principle and generalized Snell's law

Let us discuss the design of a GRIN slab in the form of the rectangular region with a gradual change of the magnetic parameters enabling the direction of the transmitted waves to be steered. To describe the wave refraction in this system, we use the Huygens-Fresnel principle [51]. This concept was developed for optics but can be adapted to other types of waves [52]. The postulation states that every point on a wavefront is itself the source of the cylindrical wavelets, and the sum of these cylindrical wavelets forms the new wavefront. In the considered case, we assume that

the source points are located at the right interface of the GRIN slab (at $x = d$) and are aligned along the y axis. We can calculate the complex amplitude at any position on the right side of the GRIN slab using the amplitude and phase shift obtained from the solution of the boundary problem. Postulation given by Huygens-Fresnel can be mathematically expressed as

$$\mathcal{T}(\mathbf{r}) = \sum_j \frac{T_j e^{i[\mathbf{k} \cdot (\mathbf{r} - \mathbf{r}_j) + \phi_j]}{|\mathbf{r} - \mathbf{r}_j|}. \quad (7)$$

The summation is done over the interface of the GRIN slab (at the position $x = d$) at a large number of locations $\mathbf{r}_j = [d, y_j]$. The phase ϕ_j is tailored by changing the saturation magnetization or anisotropy field in the GRIN slab. The partial amplitude T_j indicates the transmittance of the SW through the GRIN slab into the semi-infinite medium A defined as $\text{abs}(t_A)^2$ and the phase ϕ_j defined as $\arg(t_A)$ [Eq. (A1) in Appendix A].

Another approach for calculating the angle of the refracted wave is to use the generalized Snell law [47,53]. It states that a nonzero gradient of phase along the interface induces an additional perpendicular to the interface component of the wave vector. Mathematically it can be expressed by the following formula:

$$k_{\text{incident},y} = k_{\text{refracted},y} + \frac{d\phi}{dy}, \quad (8)$$

where ϕ is induced phase along the y axis and k_{incident} and $k_{\text{refracted}}$ are the wave numbers of the incident and refracted wave, respectively. In the case with known $\phi(y)$ dependence along the y axis, the generalized Snell law together with SW dispersion relation, can be used to predict the overall direction of the wave vector of the outgoing SWs from the GRIN slab. In our case, for normal incident waves, $k_{\text{incident},y} = 0$, therefore, $k_{\text{refracted},y} = -d\phi/dy$. The missing component of wave vector, perpendicular to the interface, can be calculated with the use of SW dispersion relation $k(\omega)$: $k_{\text{refracted},x}^2 = k^2(\omega) - k_{\text{refracted},y}^2$. Overall, the GRIN slab acts here as a metasurface. Note, that in photonics, metasurfaces can also have widths comparable to the wavelength [54].

III. RESULTS

In order to design the GRIN slab, that is schematically shown in Fig. 2, we propose to use Co-Fe-B layer as a base material due to high saturation magnetization, relatively low SW damping [55,56], which is crucial for SW processing, [57] and because of the possibility of tailoring the material parameters, required to obtain anomalous refraction.

By implantation of Ga ions, we can locally reduce the magnetization and create the distribution of saturation magnetization of high spatial resolution [46,58,59].

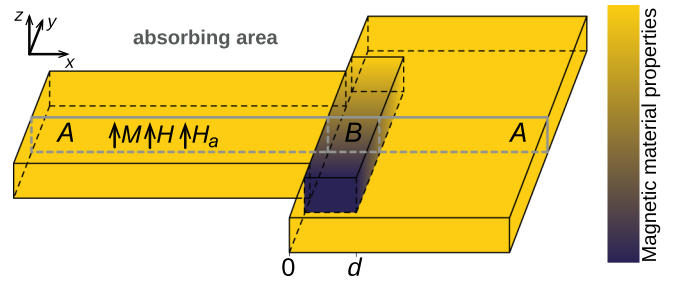


FIG. 2. Geometry of the simulation system with the GRIN element. The system consists of the ferromagnetic slab (B) characterized by the gradient of magnetic parameters (e.g., saturation magnetization M_S or anisotropy field H_a), which links the straight section of the waveguide and the semi-infinite plane made of the homogeneous material A . The magnetic parameters in the slab B are changing in the y direction. At each x - z cross section (see Fig. 1), the phase shift of transmitted wave is different, which allows refracting the plane wave propagating initially in the x direction. The absorbing material is placed at the sides of the simulated system, in order to avoid the impact of boundaries. The external magnetic field \mathbf{H} is applied along the z direction; the static magnetization and the anisotropy field are aligned with the external field.

From the other side, when the sufficiently thin layer of Co-Fe-B is deposited on MgO, the surface-induced out-of-plane anisotropy can force the perpendicular orientation of the magnetization [45,60]. The effective anisotropy field (including both the shape and surface, magnetocrystalline anisotropy) can be controlled by the annealing in the fabrication process or by the application of the electric field [61–63]. The perpendicular orientation of the magnetization ensures the isotropic SW dispersion, which simplifies the design of refraction effects. The effect of continuous change of saturation magnetization can be achieved also in a magnetic insulator, like yttrium iron garnet (YIG) by temperature [64] or strain [65].

At the initial stage, we perform the analytical studies of the SWs' transmission through the slab formed in a Co-Fe-B matrix by the modification of the saturation magnetization or the anisotropy field.

Particular attention is paid to the identification of the resonances of the slab, where the amplitude of transmitted SWs is the highest. The results are cross checked by micromagnetic simulations. Then, we present the outcomes of micromagnetic simulations for the guiding of the SWs in the waveguide with the GRIN slab at the bend. The GRIN slab is designed using the results from the initial stage and used to guide the SWs coherently through the bend of the magnonic waveguide.

A. Spin-wave propagation through the slab—one-dimensional scenario

Let us analyze the SW transmission through a uniform slab of finite width with modified either saturation

magnetization or uniaxial anisotropy field. Equations (4)–(6), with Eqs. (A1)–(A5) are taken into account to determine the phase shift $\arg(t_A)$ and the transmittance $\text{abs}(t_A)^2$ of the transmitted SWs in dependence on frequency or other considered magnetic parameters (e.g., the saturation magnetization or the anisotropy field).

To demonstrate various aspects of the system, as well as to check the validity of the model, we show the results of the analytical calculations and their comparison with the results of the micromagnetic simulations for four scenarios: (i) $M_{S,B} = 800$ kA/m in the slab is fixed, the exchange constant $A_{\text{ex},B}$ is equal to 20 pJ/m, the frequency of SWs varies in the range of 14–40 GHz and the uniaxial anisotropy is neglected, (ii) $M_{S,B} = 1200$ kA/m, $A_{\text{ex},B} = 27$ pJ/m, frequency of SWs varies in the range of 14–40 GHz and the uniaxial anisotropy $K_B = 50$ kJ/m³ is included, (iii) $M_{S,B}$ varies in the slab in the range of 300–800 kA/m, $A_{\text{ex},B} = 20$ pJ/m, frequency of SWs is 25 GHz and the uniaxial anisotropy is neglected, (iv) $M_{S,B} = 1200$ kA/m, $A_{\text{ex},B} = 27$ pJ/m, SWs frequency is 25 GHz and the uniaxial anisotropy K_B changes in the range of 0–490 kJ/m³. In all cases, the slab is 150 nm wide. Surrounding material A is assumed to be made from Co-Fe-B with $M_{S,A} = 1200$ kA/m, $A_{\text{ex},A} = 27$ pJ/m and $K_A = 0$. The external magnetic field $\mu_0 H = 0.5$ T is aligned along the z axis. Details of the micromagnetic simulations are presented in Appendix B.

We now analyze the dependence of the transmittance and phase shift of transmitted SWs on the frequency for the slab formed by the modification of saturation magnetization and uniaxial anisotropy, cases (i) and (ii). The results for these two cases are presented in Figs. 3 and 4, respectively. To explain these frequency dependencies, we should discuss the role of the transmission of exchange SWs in the SWs' dispersion relation

$$k(\omega) = \sqrt{a \left(\frac{\omega}{\omega_0} - b \right)}, \quad (9)$$

where $\omega_0 = \gamma \mu_0 H$ is proportional to the value of external field H and is expressed in the angular frequency unit, the factor $a = M_S \mu_0 H / (2A_{\text{ex}})$ is proportional to the saturation magnetization, and the term $b = 1 + H_a / H$ changes linearly with the anisotropy field $H_a = 2K / (\mu_0 M_S)$. By the change of M_S , the wave vector is scaled, regardless of the range of frequencies. However, the impact of H_a on the wave vector is significant only for low frequencies (ω is similar to ω_0) when the additive term b cannot be neglected. Moreover, for lower frequencies and sufficiently large positive value of the uniaxial anisotropy ($b > \omega / \omega_0$), the wave vector becomes imaginary and the SWs can only tunnel.

The decrease of M_S in the slab B (for A_{ex} , H , K kept constant in the system) results in the decrease of k and the reduction of the phase acquired by the transmitted

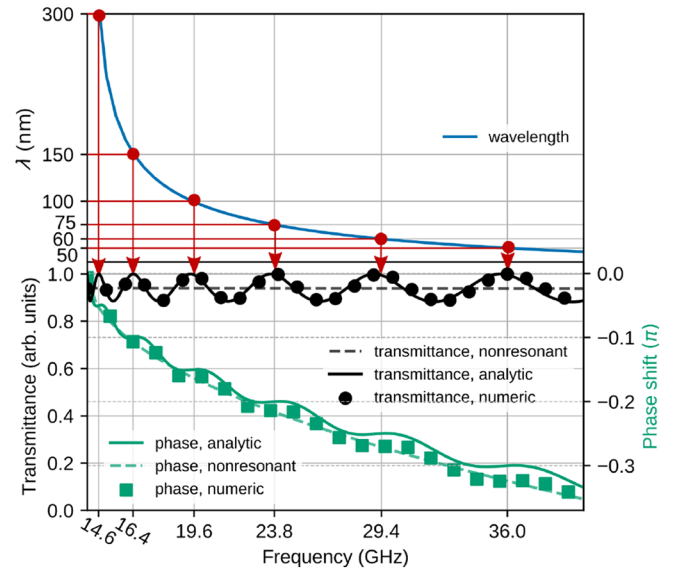


FIG. 3. SWs' wavelength (blue color) as a function of frequency. Red dots indicate fulfilled resonant conditions by Eq. (10). Enhancement of transmittance at these frequencies can be observed. Values on the horizontal axis represent the resonant frequencies. The transmittance (black color) and the phase shift (green color) for SWs traveling through the 150-nm-wide slab with respect to the frequency. Dots and squares represent the numerical simulations, while the solid lines represent the analytical results. Dashed lines represent the case when the reflection in the system is neglected. The value of the external field is equal to 0.5 T, reduced M_S in the slab is equal to 800 kA/m and reduced A_{ex} to 20 pJ/m.

SW. As a result, the phase shift is negative (referring to the SWs propagating at the same distance d in the matrix A where M_S is not reduced). This negative phase shift is growing with the increasing frequency $\Delta\varphi(\omega) = d[k(\omega, M_{S,B}) - k(\omega, M_{S,A})]$ —see green lines and points in Fig. 3, because $k(\omega)$ is an increasing function of the frequency. The increase of the anisotropy field H_a in the slab B reduces the value of k . Therefore, the SWs gain additional phase during the transmission through the slab (referring to the SWs propagating at the same distance in the matrix A where H_a are not added). This positive phase shift is growing (see green lines and points in Fig. 4) for the same reasons as in the case of the slab formed by the change of M_S .

It is visible that the value of transmittance oscillates. It is especially noticeable in the case of the slab induced by the M_S reduction, Fig. 3. To explain this behavior, the dispersion relations of SWs as the dependencies of wavelength on frequency $\lambda(\omega) = 2\pi/k(\omega)$ are plotted in Figs. 3 and 4 [cf. Eq. (9)]. The resonance condition for wave transmitted through the slab of the width d reads

$$2d = N\lambda(\omega), \quad (10)$$

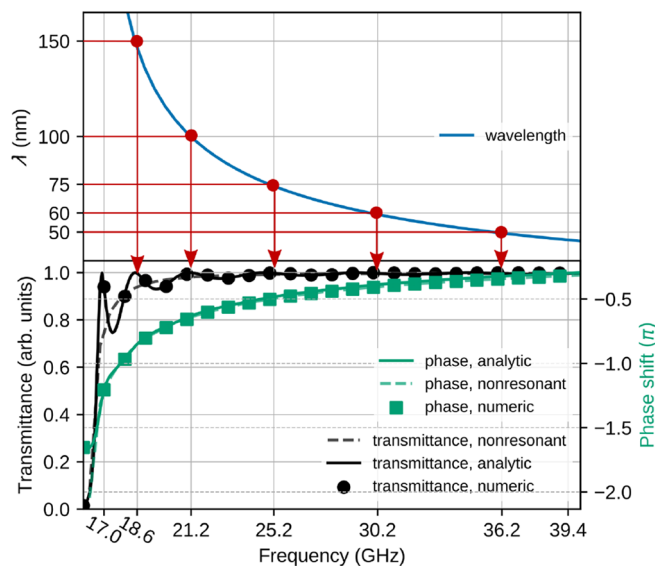


FIG. 4. SWs' wavelength (blue color) as a function of frequency. Red dots indicate fulfilled resonant conditions, Eq. (10), where we observe an enhancement of the transmittance. Values on the horizontal axis represent the resonant conditions. Transmittance (black color) and phase shift (green color) for SWs propagating through the 150-nm-wide slab with respect to the frequency. Dots and squares represent the values obtained in numerical simulation, while the solid lines represent the analytical results. Dashed lines represent the case when the reflection in the system is neglected. The value of the external field is equal to 0.5 T and the uniaxial anisotropy constant $K = 5 \text{ kJ/m}^3$ within the slab.

where N is the natural number. The condition Eq. (10) corresponds to the constructive interference of the wave after the round trip at a distance of $2d$. The frequencies for these resonances are marked in Figs. 3 and 4 by the red arrows. They match the locations of the maxima of the transmittance. In order to confirm the presence of standing resonance modes within the slab, we perform both the analytical calculations and micromagnetic simulations. We calculate the squared dynamical magnetization, averaged in time, at the frequencies corresponding to the maxima of the transmission. It can be observed that the slab works as a resonator (see the results in Appendix A), similar to Fabry-Perot resonators known in optics [51]. It is worthwhile to note, that the fabrication of the sharp interfaces between the GRIN slab and its surrounding might be problematic, especially when one would like to use the ion implantation to shape the distribution of saturation magnetization within the sample. The effect of a smooth transition between the slab and surrounding is important for the sharpness of resonances, but it does not affect significantly the phase shift acquired by the SW.

One can predict the phase shift, which SWs gain during the transmission through the slab, by defining a magnonic

refractive index [37,66]. However, this approach takes into account only the refractive properties of the bulk material expressed in the dispersion relation. By solving the LLE [Eq. (1)] with clearly defined boundary conditions [Eqs. (2) and (3)], we can obtain full information about the SWs' refraction in the system. Hence, we can see in Figs. 3 and 4 the corrections, which come from taking into account the reflection from boundaries. The dashed lines with a lighter color indicate the cases when no reflection is considered in the system. As we can see, even for strong exchange coupling (when the majority of energy is transmitted for any condition) at the interface, A , the difference is noticeable. For weaker coupling, where a more significant fraction of energy is turned back, the impact on the phase shift and the transmittance could be even more significant [45]. This points out that the design of the GRIN slab has to take into account the presence of the resonances.

Numerical calculations fully support the analytical approach presented in this part, and thus the validated model is used for further stages of this study.

Let us now discuss cases (iii) and (iv), described at the beginning of the section. Here, we aim to control the SW guiding in the confined structures like waveguides using the GRIN slab, so in the following we introduce the change of the material parameters, saturation magnetization M_S and the anisotropy field H_a . According to Fig. 2, we change the material parameters of the slab at fixed frequency of SWs $f = \omega/(2\pi) = 25 \text{ GHz}$.

In Fig. 5(a), the transmittance and the phase shift with respect to M_S in the slab are presented. The resonant phenomenon is visible, like in the previous cases. The modulation of the transmittance is around 20%. The dashed black line represents the transmittance of SWs through the slab when the reflection is neglected. The impact of the resonances is visible, and taking into account the resonant effect is well based. The phase shift changes rather smoothly in the considered range of M_S , and in total, the difference is around 1.75π . Deviations of the green solid and squared lines (analytical and numerical results, respectively) from the dashed line are minor and visible mainly near the resonances. Fig. 5(b) shows the results for the transmittance and phase shift as a function of the anisotropy constant K in the slab in the range of 0–490 kJ/m^3 , which is equivalent to the presence of the anisotropy field $\mu_0 H_a$ in the range 0–0.8 T.

We can see that for the anisotropy field larger than 0.4 T, the transmittance drops dramatically, and the resonance peaks are not observed anymore. This feature is attributed to the lack of oscillating solution within the slab. The SWs need to tunnel through the slab with a significant reduction of the amplitude. Just below this value [$H_a = 2\pi/(\gamma\mu_0)f - H$], the resonant behavior of the transmittance is observed with a high variation of the transmittance.

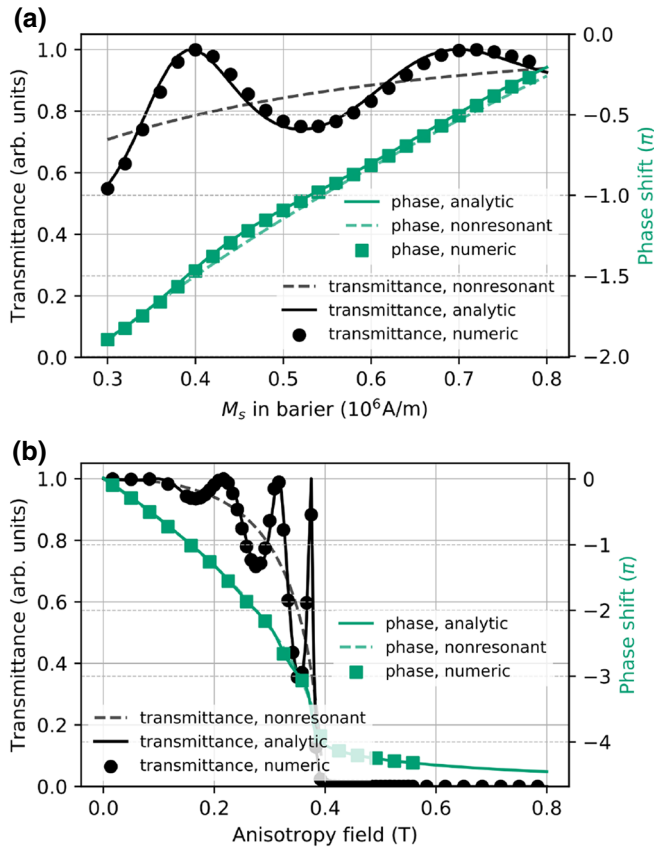


FIG. 5. Transmittance (black color) and phase shift (green color) for SWs traveling through the 150-nm-wide slab with respect to (a) M_S and (b) the anisotropy field in the slab. Dots and squares represent the values obtained in numerical simulation, while the solid lines represent the analytical results. Dashed lines represent the nonresonant case. The constant frequency equal to 25 GHz and external field equal to 0.5 T are considered. (a) The reduced exchange A_{ex} is equal to 20 pJ/m. Resonant peaks are visible for the specific values of M_S . (b) M_S and A_{ex} remain the same as in the matrix, i.e., 1200 kA/m and 27 pJ/m, respectively.

B. Anomalous refraction of spin waves

Based on the model developed in Sec. II, we design a GRIN slab that bends wavefronts of the incident waves in the desired way. The slab is an element that modifies the phase of the incoming plane waves (at the interface located in $x = 0$) to gain the linear change of the phase of the transmitted waves alongside the interface (at $x = d$). This idea is based on the general concept of tailoring the phase changes alongside the interface and provide the desired functionality, like focusing [44], beam steering or delay [67]. In the present case, we want to design an element suitable for the change of the direction of SWs' propagation. Let us study numerically the case of the two-dimensional slab with the gradient of M_S , like it is schematically presented in Fig. 2. In the section of the straight and flat waveguide of the width 100 nm, we excite

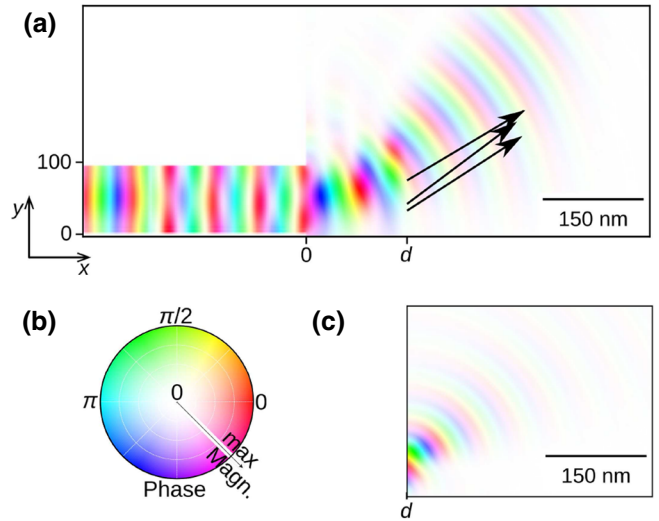


FIG. 6. The squared amplitude of SWs propagating in the system shown in Fig. 2, at the frequency 25 GHz. (a) When SWs reach the semi-infinite medium after the slab, the new wavefront starts to form due to the gradient of magnetic parameters. The bending of SWs reaches the angle of ca. 36° . (b) The color palette of SW. The color indicates the phase, while the intensity indicates the amplitude. (c) The bending of SWs ca. 36° obtained according to the Huygens-Fresnel formula [Eq. (7)]. Source points of cylindrical SWs are located on the right border of the slab—at the position d . The amplitude of the transmittance and the phase shift are obtained from the boundary-condition problem, like in Fig. 5(a).

the plane wave, which propagates along the x axis. The waveguide is attached to the large plate of the same thickness and made of the same material. At the front of the plate, we defined the 150-nm-wide slab—see Fig. 2. In the slab, we take the reduced value of M_S , which is increasing from 300 kA/m up to 800 kA/m on the distance 100 nm, in direct contact with the waveguide. Above M_S goes to the value of a semi-infinite plane, it is $M_S = 1200$ kA/m.

The results of the numerical simulations are presented in Fig. 6(a). The wavefront changes the direction, and the outgoing SWs are bent. The arrows in Fig. 6(a) indicate the direction of the refracted waves estimated with Eq. (8). Although the gradient of the phase shift is not perfectly linear, this estimation seems to be very good.

The results of the numerical simulations are also compared to the results of the analytical consideration using the Huygens-Fresnel principle. Complex amplitudes at every position are calculated according to the postulation given by Eq. (7). We assume that at the position d [as it is shown in Fig. 6(c)], we have a line of sources of cylindrical waves. Figure 5(a) presents the transmittance and phase shift of the SW that we need to put into Eq. (7). The application of this equation is shown in Fig. 6(c). Since the phase shift changes smoothly along the y axis, the wavefront of the SWs transmitted through the slab is reconstructed in a

way so that we observe the bending of SWs of approximately 36° . We can conclude that the procedure based on the Huygens-Fresnel principle and the approach based on the generalized Snell law are suitable for the estimation of the results of the numerical simulation, and these analytical approaches can describe the system.

C. Graded index slab at the bend of the magnonic waveguide

We use the GRIN slab, designed in the previous section, to guide the SWs through the bend of the waveguide. The numerical study is performed with the aid of micromagnetic simulations (see Appendix B).

Let us consider two straight sections of the flat waveguides of the width 100 nm, made of Co-Fe-B, and connected at the angle 36° . At this angle, we observe the refraction of the SWs by the GRIN slab with the assumed gradient of the saturation magnetization (Fig. 6). In Fig. 7(a), we present this curved waveguide with such a GRIN slab placed at the bend, whereas the results for SWs' propagation through the same structure without the GRIN element are presented in Fig. 7(b). These two systems guide the SWs differently. We can see the SWs' interference pattern in the outgoing section of the bent waveguide without the GRIN slab. Such behavior results from the scattering of the incident fundamental mode (not quantized across the waveguide's width) to the higher modes (quantized across the waveguide's width). As a consequence, the information encoded into the phase of the incident fundamental mode is lost. On the other hand, the application of the GRIN slab introduces the anomalous refraction at waveguide's bend causing that the outgoing waves to propagate along the waveguide in the form of the fundamental mode with nondisturbed wavefronts and well-defined phase. The details of the shape of the bend are irrelevant as long as its geometry follows the rotation of the SW's wavefront in graded index material.

In the previous calculations, the dipolar interactions are neglected, since their full consideration in the boundary-condition problem is a complicated task. Therefore, all investigations are limited to the exchange SWs, including the micromagnetic simulations. Such an approach is justified because the exchange interactions dominate over the dipolar ones for short-wavelength SWs. However, in order to verify the applicability of the GRIN slab, we perform simulations that also include dipolar interactions.

Let us discuss the waveguide with a GRIN slab in which the gradient of the anisotropy field is introduced. In this scenario, the static dipolar magnetic field is uniform throughout the whole system, i.e., if $H > M_S$, like in our system, $\mathbf{H}_{\text{dem},0} = -\hat{\mathbf{z}}M_S$, since the saturation magnetization is uniform, which makes the system easier to model. Following Fig. 5(b), we choose the range of anisotropy, which needs to be applied to have the same bending of

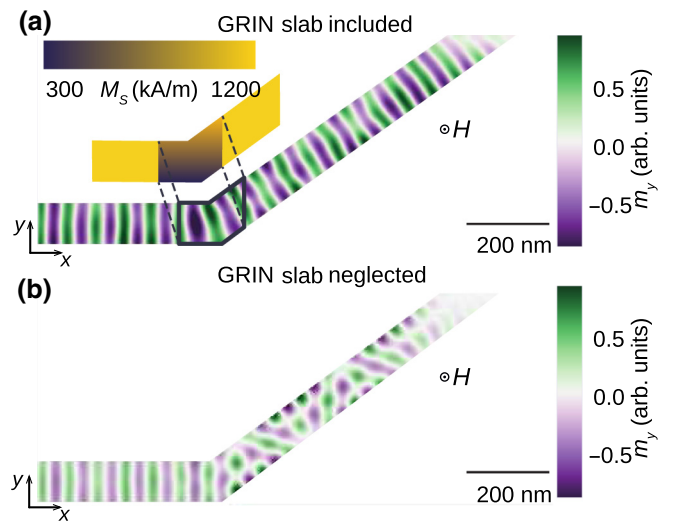


FIG. 7. (a) Propagation of SWs in the Co-Fe-B waveguide, where the GRIN slab is placed at the bend, releases the anomalous refraction. The GRIN slab has the same gradient of M_S as used in Fig. 6. The color map represents a dynamical component of the magnetization in the y direction. A snapshot is taken at the moment when a steady state is reached. At the beginning of the horizontal branch of the waveguide, the microwave antenna excites the SWs and at the end of the tilted branch, the SWs are damped to avoid any reflection. After taking a turn, the SWs propagate smoothly. (b) SWs' propagation in the waveguide without a gradient of magnetic parameters. After taking a turn, the SWs show a complex behavior due to interference between different modes of the waveguide. The width of the waveguide is 100 nm. The material parameters are the same as for the system presented in Fig. 6.

SWs, as for the studies presented in Fig. 7. Keeping the same shape of the GRIN slab, we choose the gradient of the uniaxial anisotropy field in the range from 0.27 to 0 T. The results are compared with the case when the dipolar interactions are included in the micromagnetic simulations, for the same geometry and the values of magnetic parameters. For the 100-nm-wide and 5-nm-thick waveguide, the static demagnetizing field shifts down the dispersion relation, so in order to keep the same wave vector for the considered frequency (25 GHz), it is necessary to apply the external magnetic field of increased value with respect to simulations without the dipolar interactions. We analyze the dispersion relations and find that an additional field $\mu_0 H = 1.35$ T compensates the effect of the static demagnetizing field. The cases when the dipolar interaction is taken into account or neglected, are compared in Fig. 8. Only a small difference is visible, which means that the impact of the dipolar field is not significant. The difference results from different boundary conditions at the edges of waveguides, where spins are partially pinned [68].

It is necessary to note, that in the case of the GRIN slab with the gradient of saturation magnetization in the

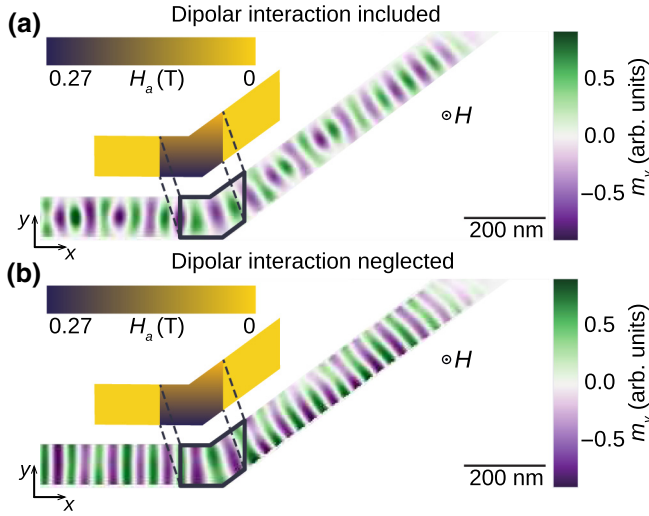


FIG. 8. SW propagation in the bent waveguide of the same geometry, as in Fig. 7. The GRIN slab placed at the bend is characterized by the gradient of anisotropy field H_a . The gradient of H_a is chosen to obtain refraction at the same angle, as in Fig. 7. In (a) the dipolar interaction is included and in (b) it is neglected in the micromagnetic simulations.

out-of-plane magnetized thin film, the static demagnetizing field is not uniform. As a result, both the saturation magnetization and static effective magnetic field are changed in parallel, and it also needs to be taken into account in the design of the GRIN slab for SW steering, which is out of the scope of this paper.

IV. SUMMARY

We present a comprehensive study of the SWs' propagation through the GRIN slab with spatially modulated saturation magnetization or uniaxial anisotropy. Using the analytical model, cross checked by numerical simulations, we are able to relate the phase acquired by SWs during the transmission through the GRIN slab at different locations to the values of the spatially dependent magnetic parameters. With this knowledge, we design the GRIN slab, ensuring the phase-coherent refraction of SWs at a desirable angle, determined by the gradient of saturation magnetization or the gradient of the anisotropy field. Notably, the presented GRIN slab enabled a wide range of phase changes (ca. 1.75π) for high and uniform transmission of SWs (transmittance in the range of 80%–100%) enhanced by utilizing the Fabry-Perot resonances. The analytical model and the main numerical demonstrations are performed for the exchange SWs, later validated with micromagnetic simulations for selected cases with included dipolar interactions.

As an application, we demonstrate the GRIN slab used to guide the SWs coherently in fundamental mode

along the bend in a magnonic waveguide. The micromagnetic simulations are performed for realistic structure and showed the possibility for experimental realization of this idea.

The GRIN slab considered in this paper can be activated on demand by the voltage-induced anisotropy [63]. The spatial changes of the perpendicular anisotropy can be introduced by the variation of the thickness of an insulating spacer separating one of the electrodes. This can open the route for voltage-controlled routing of SWs.

The proposed approach can be verified experimentally by state-of-the-art techniques, like x-ray magnetic circular dichroism [22,69], phase-resolved Brillouin-light-scattering [70], or broadband-microwave spectroscopy [46,71]. We believe that our findings are substantial for further development of the circuits for analog and digital computing based on SWs and contribute to the field of magnonics.

ACKNOWLEDGMENTS

Szymon Mieszczak and Oksana Busel contributed equally to this work.

The study has received financial support from the National Science Centre of Poland Grant No. UMO-2016/21/B/ST3/00452 and support from the EU – Horizon 2020 project MagIC Grant No. 644348.

APPENDIX A: SPATIAL PROFILES OF THE SPIN WAVES, RESONANTLY SCATTERED AT THE MAGNETIC SLAB

Solution of the LLE, Eq. (1), provides information about the complex amplitudes of SWs, which propagate in the system. The one-dimensional model presented in this paper has the following solutions:

$$t_A = \frac{4e^{id(k_B - k_A)}}{\alpha_A \alpha_B k_A k_B [(f^+)^2 - e^{2idk_B} (f^-)^2]}, \quad (\text{A1})$$

$$r_A = \frac{-(f^-)^* f^+ + e^{2idk_B} (f^+)^* f^-}{[(f^+)^2 - e^{2idk_B} (f^-)^2]}, \quad (\text{A2})$$

$$t_B = \frac{2f^+}{\alpha_B k_B [(f^+)^2 - e^{2idk_B} (f^-)^2]}, \quad (\text{A3})$$

$$r_B = \frac{2e^{2idk_B} f^-}{\alpha_B k_B [(f^+)^2 - e^{2idk_B} (f^-)^2]}, \quad (\text{A4})$$

where f^\pm is an auxiliary function, namely

$$f^\pm = \frac{M_B}{\alpha_A M_A k_A} \pm \frac{M_A}{\alpha_B M_B k_B} - \frac{i}{A},$$

and $(f^\pm)^*$ is its complex conjugate. The dependence of the wave number on angular frequency $k_{A(B)}(\omega)$ expresses the dispersion relation:

$$k_{A(B)} = \frac{1}{\sqrt{\alpha_{A(B)} M_{S,A(B)}}} \sqrt{\frac{\omega}{\gamma} - \mu_0 [H + H_{a,A(B)}]}, \quad (\text{A5})$$

where H and $H_{a,A(B)}$ are external and anisotropy fields, respectively.

Parameter δ is the thickness of the interfaces and it is a fitting parameter. We find that the best match between analytical and numerical results is achieved for the value of $\delta = 0.5$ nm. It is a reasonable value since the size of the unit cell in micromagnetic simulations is 1 nm.

Information about the energy flow (the amplitude of SWs) and phase shifts can be extracted from Eqs. (A1)–(A4), and as we can see in Figs. 3–5, both quantities fit perfectly to micromagnetic simulations.

Let us present the spatial profile of dynamical components of the magnetization vector. Set of Eqs. (4)–(6), with coefficients defined in Eqs. (A1)–(A4), describe the analytical solution of SW in complex form. To visualize these spatial profiles, the magnetization should be presented in the real form:

$$m = \text{Re} [\tilde{m} e^{i(kx - \omega t)}] = |\tilde{m}| \cos(kx - \omega t + \arg \tilde{m}), \quad (\text{A6})$$

where \tilde{m} is a complex coefficient defined for a specific region. It can be incidence, reflection, or transmission coefficient, as defined in Eqs. (A1)–(A4).

In order to compare the results of the analytical model with the ones from numerical simulations, we need to get rid of the explicit dependence on time, because we are not able to compare some exact moments in time. Hence, we average the squared magnetization component in time. The same as we did with the output from simulation after reaching a steady state. The comparison is shown in Fig. 9. We plot the spatial profile of SW for five specific frequencies (see Fig. 3), Figs. 9(a)–9(e), where transmittance is equal to 1 (see Fig. 3). Dark background represents the slab B . Standing wave is visible, which indicates the existence of resonant effect in accordance with Eq. (10). The slab is coupled to the surrounding, and the transmission is relatively high. Therefore, the nodes are not located at zero level, because the amplitude of the reflected wave is always lower than the amplitude of the incident wave. On the right areas (light background), SWs are propagating with a constant amplitude, so after averaging, we get a straight line. Its level indicates the energy flow.

Figure 9 is another remarkable confirmation of the validity of our analytical model.

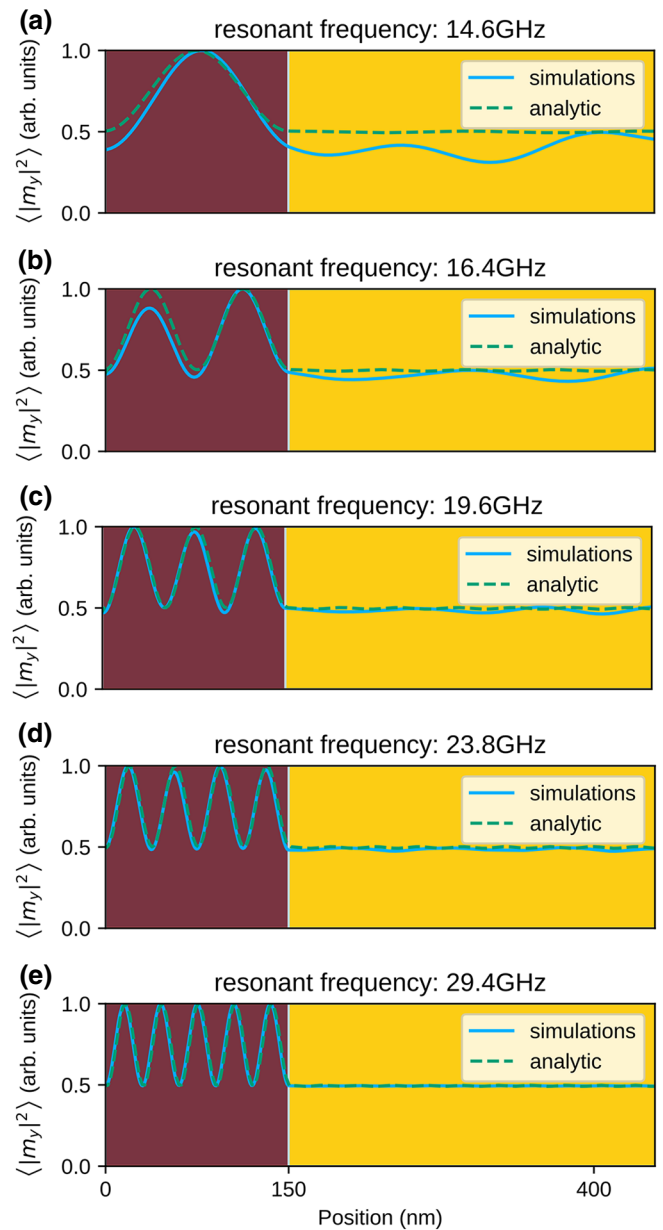


FIG. 9. Normalized spatial profile of dynamical component of the magnetization for the five lowest resonances (a) 14.6 GHz, (b) 16.4 GHz, (c) 19.6 GHz, (d) 23.8 GHz, and (e) 29.4 GHz. Width of the slab is 150 nm, M_S in the matrix is 1200 kA/m and $A_{\text{ex}} = 28$ pJ/m. External field is 0.5 T, reduced M_S within the slab is 800 kA/m and reduced exchange stiffness constant A_{ex} is 20 pJ/m. The presented resonances correspond to Fig. 3.

APPENDIX B: MICROMAGNETIC SIMULATIONS

The micromagnetic simulations are performed with the use of the mumax3 package [72], which is the finite-difference time-domain solver of the full Landau-Lifshitz equation. The simulations are conducted to (i) calculate the transmittance and the phase shift of the waves transmitted through the one-dimensional slab, (ii) demonstrate anomalous refraction in thin film, and finally, (iii) to demonstrate

a slab suitable for SW bending in magnonic waveguides. In all these cases, the steady state is simulated, i.e., the response of the system after long, continuous excitation of SWs at a single frequency enabling SWs to travel to the sides of the simulated system.

In order to neglect the influence of the reflections from the borders of the simulated system and, therefore, simplify interpretation of the results, the absorbing boundary conditions are implemented around the sides of the simulated domain (see Fig. 2). In all the simulations we consider SW propagation in 5-nm-thick Co-Fe-B film ($M_S = 1200$ kA/m, $A_{\text{ex}} = 27$ pJ/m and reduced damping to 0.0001) in the presence of the out-of-plane magnetic field (applied along the z axis) of value $\mu_0 H = 0.5$ T and discretized with cuboid elements of dimensions ($1 \times 1 \times 5$ nm³). These values are comparable to the exchange length. Magnetic parameters are modulated only in the region of the slab described in the main part of the paper. In order to be consistent with the analytical theory, which neglects the dipolar interactions, most of the simulations are performed with neglected dipolar interactions as well. Nevertheless, in order to further validate this model, a set of micromagnetic simulations with included dipolar interaction is performed to demonstrate the applicability of the considered slabs to bend SW in a curved waveguide (see Fig. 8).

To calculate the transmittance and the phase shift of the transmitted SW through the slab with respect to frequency or various magnetic parameters, we define a one-dimensional geometry, i.e., discretized by $L_x \times L_y \times L_z$ ($4096 \times 1 \times 1$) unit cells. These values are obtained by running two separate simulations, i.e., a reference simulation without the slab, and the additional one with the slab. Then, the results of these simulations are compared in order to extract the values of transmittance and phase shift. The transmittance was calculated as a ratio of squared amplitude and the phase shift—as a difference of the SW phases. SWs are excited by an rf magnetic field of frequencies in the range of 14–40 GHz for fixed material parameters or 25 GHz for various material parameters of the slab. rf field is applied locally in a 6-nm narrow region, located on the left side of the slab at a distance of 1548 nm from the slab.

To demonstrate an anomalous refraction in action, we define a two-dimensional system discretized by $L_x \times L_y \times L_z$ ($1024 \times 1024 \times 1$) unit cells. The scheme of the system is presented in Fig. 2. SWs are excited by an rf field of frequency 25 GHz applied locally in a 6-nm narrow region located on the left side of the slab in the distance of 232 nm. Three different areas can be distinguished there. On the left is the narrow part, 100-nm-wide waveguide, which introduces SWs into the system. In the middle is a 100-nm-wide and 150-nm-long slab with a gradient of the magnetic parameters. The gradient of the magnetic parameters is induced along the y axis.

Saturation magnetization changes in the range of 300–800 kA/m on the distance 100 nm, with direct contact with waveguide. Above is smoothly changed in the range of 800–1200 kA/m to avoid sharp edges. Below, a constant value of 300 kA/m is assumed. On the right-hand side is the semi-infinite medium, which allows the propagation of SWs in any direction freely.

Finally, using the knowledge from the previous step, we design a curved waveguide, which supports coherent SW propagation alongside the waveguide. To create such a curved waveguide, we cut the finite two-dimensional system following the newly created wavefront. The system is discretized by $L_x \times L_y \times L_z$ ($2048 \times 512 \times 1$) unit cells. SWs are excited by an rf magnetic field of frequency 25 GHz applied locally in 6-nm narrow region located at the distance of 224 nm to the corner from the left side.

-
- [1] S. O. Demokritov and A. N. Slavin, *Magnonics – From Fundamentals to Applications* (Springer-Verlag, Berlin, Heidelberg, 2013).
 - [2] G. Csaba, Adám Papp, and W. Porod, Perspectives of using spin waves for computing and signal processing, *Phys. Lett. A* **381**, 1471 (2017).
 - [3] A. Khitun, Magnonic holographic devices for special type data processing, *J. Appl. Phys.* **113**, 164503 (2013).
 - [4] A. Khitun, M. Bao, and K. L. Wang, Magnonic logic circuits, *J. Phys. D: Appl. Phys.* **43**, 264005 (2010).
 - [5] A. V. Chumak, in *Spintronics Handbook: Spin Transport and Magnetism* (CRC Press, 2019), 2nd ed.
 - [6] K. Vogt, F. Fradin, J. Pearson, T. Sebastian, S. Bader, B. Hillebrands, A. Hoffmann, and H. Schultheiss, Realization of a spin-wave multiplexer, *Nat. Commun.* **5**, 3727 (2014).
 - [7] A. V. Sadovnikov, C. S. Davies, V. V. Kruglyak, D. V. Romanenko, S. V. Grishin, E. N. Beginin, Y. P. Sharaevskii, and S. A. Nikitov, Spin wave propagation in a uniformly biased curved magnonic waveguide, *Phys. Rev. B* **96**, 060401 (2017).
 - [8] K. Vogt, H. Schultheiss, S. Jain, J. Pearson, A. Hoffmann, S. Bader, and B. Hillebrands, Spin waves turning a corner, *Appl. Phys. Lett.* **101**, 042410 (2012).
 - [9] A. Haldar, D. Kumar, and A. O. Adeyeye, A reconfigurable waveguide for energy-efficient transmission and local manipulation of information in a nanomagnetic device, *Nat. Nanotechnol.* **11**, 437 (2016).
 - [10] D. D. Sheka, O. V. Pylypovsky, P. Landeros, Y. Gaididei, A. Kakay, and D. Makarov, Micromagnetic theory of curvilinear ferromagnetic shells, arXiv:1904.02641v1 (2019).
 - [11] Y. Gaididei, A. Goussev, V. P. Kravchuk, O. V. Pylypovskyi, J. M. Robbins, D. D. Sheka, V. Slastikov, and S. Vasylyevych, Magnetization in narrow ribbons: curvature effects, *J. Phys. A* **50**, 385401 (2017).
 - [12] V. S. Tkachenko, A. N. Kuchko, M. Dvornik, and V. V. Kruglyak, Propagation and scattering of spin waves in curved magnonic waveguides, *Appl. Phys. Lett.* **101**, 152402 (2012).

- [13] Q. Wang, B. Heinz, R. Verba, M. Kewenig, P. Pirro, M. Schneider, T. Meyer, B. Lagel, C. Dubs, T. Bracher, and A. V. Chumak, Spin Pinning and Spin-Wave Dispersion in Nanoscopic Ferromagnetic Waveguides, *Phys. Rev. Lett.* **122**, 247202 (2019).
- [14] V. E. Demidov, M. P. Kostylev, K. Rott, J. Munchenberger, G. Reiss, and S. O. Demokritov, Excitation of short-wavelength spin waves in magnonic waveguides, *Appl. Phys. Lett.* **99**, 082507 (2011).
- [15] C. Liu, J. Chen, T. Liu, F. Heimbach, H. Yu, Y. Xiao, J. Hu, M. Liu, H. Chang, T. Stueckler, S. Tu, Y. Zhang, Y. Zhang, P. Gao, Z. Liao, D. Yu, K. Xia, Na Lei, W. Zhao, and M. Wu, Exchange-torque-induced excitation of perpendicular standing spin waves in nanometer-thick YIG films, *Nat. Commun.* **4**, 2702 (2018).
- [16] S. J. Hamalainen, F. Brandl, K. J. A. Franke, D. Grundler, and S. van Dijken, Tunable Short-Wavelength Spin-Wave Emission and Confinement in Anisotropy-Modulated Multiferroic Heterostructures, *Phys. Rev. Appl.* **8**, 014020 (2017).
- [17] J. Chen, T. Yu, C. Liu, T. Liu, M. Madami, K. Shen, J. Zhang, S. Tu, M. S. Alam, K. Xia, M. Wu, G. Gubbiotti, Y. M. Blanter, G. E. W. Bauer, and H. Yu, Excitation of unidirectional exchange spin waves by a nanoscale magnetic grating, *Phys. Rev. B* **100**, 104427 (2019).
- [18] F. Fohr, A. A. Serga, T. Schneider, J. Hamrle, and B. Hillebrands, Phase sensitive Brillouin scattering measurements with a novel magneto-optic modulator, *Rev. Sci. Instrum.* **80**, 043903 (2009).
- [19] S. J. Hamalainen, M. Madami, Q. Huajun, G. Gubbiotti, and S. van Dijken, Control of spin-wave transmission by a programmable domain wall, *Nat. Commun.* **9**, 4853 (2018).
- [20] J. Jersch, V. E. Demidov, H. Fuchs, K. Rott, P. Krzyteczko, J. Munchenberger, G. Reiss, and S. O. Demokritov, Mapping of localized spin-wave excitations by near-field Brillouin light scattering, *Appl. Phys. Lett.* **97**, 152502 (2010).
- [21] G. Dieterle, J. Forster, H. Stoll, A. S. Semisalova, S. Finizio, A. Gangwar, M. Weigand, M. Noske, M. Fahnle, I. Bykova, J. Grafe, D. A. Bozhko, H. Y. Musienko-Shmarova, V. Tiberkevich, A. N. Slavin, C. H. Back, J. Raabe, G. Schutz, and S. Wintz, Coherent Excitation of Heterosymmetric Spin Waves with Ultrashort Wavelengths, *Phys. Rev. Lett.* **122**, 117202 (2019).
- [22] J. Grafe, M. Weigand, B. V. Waeyenberge, A. Gangwar, F. Gro, F. Lisiecki, J. Rychy, H. Stoll, N. Trager, J. Forster, F. Stobiecki, J. Dubowik, J. Kos, M. Krawczyk, C. H. Back, E. J. Goering, and G. Schutz, in *Spintronics XIII*, edited by H.-J. M. Drouhin, J.-E. Wegrowe, and M. Razeghi, Visualizing nanoscale spin waves using MAXYMUS, *Proc. SPIE* **11090**, 1109025 (2019).
- [23] F. Garcia-Sanchez, P. Borys, R. Soucaille, J.-P. Adam, R. L. Stamps, and J.-V. Kim, Narrow Magnonic Waveguides Based on Domain Walls, *Phys. Rev. Lett.* **114**, 247206 (2015).
- [24] K. Wagner, A. Kakay, K. Schultheiss, A. Henschke, T. Sebastian, and H. Schultheiss, Magnetic domain walls as reconfigurable spin-wave nanochannels, *Nat. Nanotechnol.* **11**, 432 (2016).
- [25] C. Banerjee, P. Gruszecki, J. W. Klos, O. Hellwig, M. Krawczyk, and A. Barman, Magnonic band structure in a Co/Pd stripe domain system investigate by Brillouin light scattering and micromagnetic simulations, *Phys. Rev. B* **96**, 024421 (2017).
- [26] J. Lan, W. Yu, R. Wu, and J. Xiao, Spin-Wave Diode, *Phys. Rev. X* **5**, 041049 (2015).
- [27] Y. Henry, D. Stoeffler, J.-V. Kim, and M. Bailleul, Unidirectional spin-wave channeling along magnetic domain walls of Bloch type, *Phys. Rev. B* **100**, 024416 (2019).
- [28] P. Gruszecki, C. Banerjee, M. Mruczkiewicz, O. Hellwig, A. Barman, and M. Krawczyk, in *Solid State Physics* (Elsevier, 2019), Vol. 70, p. 79.
- [29] E. Albisetti, D. Petti, G. Sala, R. Silvani, S. Tacchi, S. Finizio, S. Wintz, A. Cal, X. Zheng, J. Raabe, E. Riedo, and R. Bertacco, Nanoscale spin-wave circuits based on engineered reconfigurable spin-textures, *Comm. Phys.* **1**, 56 (2018).
- [30] P. Clausen, K. Vogt, H. Schultheiss, S. Schafer, B. Obry, G. Wolf, P. Pirro, B. Leven, and B. Hillebrands, Mode conversion by symmetry breaking of propagating spin waves, *Appl. Phys. Lett.* **99**, 162505 (2011).
- [31] J. W. Klos, D. Kumar, M. Krawczyk, and A. Barman, Influence of structural changes in a periodic antidot waveguide on the spin-wave spectra, *Phys. Rev. B* **89**, 014406 (2014).
- [32] S. Pan, J. W. Klos, S. Mieszczak, A. Barman, and M. Krawczyk, Spin waves in periodic antidot waveguide of complex base, *J. Phys. D: Appl. Phys.* **50**, 275003 (2017).
- [33] K.-S. Lee, D.-S. Han, and S.-K. Kim, Physical Origin and Generic Control of Magnonic Band Gaps of Dipole-Exchange Spin Waves in Width-Modulated Nanostrip Waveguides, *Phys. Rev. Lett.* **102**, 127202 (2009).
- [34] F. Ciubotaru, A. V. Chumak, N. Y. Grigoryeva, A. A. Serga, and B. Hillebrands, Magnonic band gap design by the edge modulation of micro-sized waveguides, *J. Phys. D: Appl. Phys.* **45**, 255002 (2012).
- [35] J.-N. Toedt, M. Mundkowsky, D. Heitmann, S. Mendach, and W. Hansen, Design and construction of a spin-wave lens, *Sci. Rep.* **6**, 33169 (2016).
- [36] C. S. Davies, A. Francis, A. V. Sadovnikov, S. V. Chertopalov, M. T. Bryan, S. V. Grishin, D. A. Allwood, Y. P. Shararevskii, S. A. Nikitov, and V. V. Kruglyak, Towards graded-index magnonics: Steering spin waves in magnonic networks, *Phys. Rev. B* **92**, 020408 (2015).
- [37] M. Vogel, B. Hillebrands, and G. Freymann, Spin-Wave Optical Elements: Towards Spin-Wave Fourier Optics, arXiv:1906.02301 (2019).
- [38] P. Gruszecki and M. Krawczyk, Spin-wave beam propagation in ferromagnetic thin films with graded refractive index: Mirage effect and prospective applications, *Phys. Rev. B* **97**, 094424 (2018).
- [39] N. J. Whitehead, S. A. R. Horsley, T. G. Philbin, and V. V. Kruglyak, A Luneburg lens for spin waves *Appl. Phys. Lett.* **113**, 212404 (2018).
- [40] N. J. Whitehead, S. A. R. Horsley, T. G. Philbin, and V. V. Kruglyak, Graded index lenses for spin wave steering, *Phys. Rev. B* **100**, 094404 (2019).
- [41] R. Gieniusz, P. Gruszecki, M. Krawczyk, U. Guzowska, A. Stognij, and A. Maziewski, The switching of strong spin wave beams in patterned garnet films, *Sci. Rep.* **7**, 8771 (2017).
- [42] O. Dzyapko, I. Borisenko, V. Demidov, W. Pernice, and S. Demokritov, Reconfigurable heat-induced spin wave lenses, *Appl. Phys. Lett.* **109**, 232407 (2016).

- [43] M. Vogel, R. Aßmann, P. Pirro, A. V. Chumak, B. Hillebrands, and G. von Freymann, Control of Spin-Wave Propagation using Magnetisation Gradients, *Sci. Rep.* **8**, 1 (2018).
- [44] M. Zelent, M. Mailyan, V. Vashista, P. Gruszecki, O. Gorobets, Y. Gorobets, and M. Krawczyk, Spin wave collimation using a flat metasurface, *Nanoscale* **11**, 9743 (2019).
- [45] J. W. Kłos, Y. S. Dadoenkova, J. Rychły, N. N. Dadoenkova, I. L. Lyubchanskii, and J. Barnaś, Hartman effect for spin waves in exchange regime, *Sci. Rep.* **8**, 17944 (2018).
- [46] O. V. Dobrovolskiy, R. Sachser, S. A. Bunyaev, D. Navas, V. M. Bezv, M. Zelent, W. Śmigaj, J. Rychły, M. Krawczyk, R. V. Vovk, M. Huth, and G. N. Kakazei, Spin-Wave Phase Inverter upon a Single Nanodefekt, *ACS Appl. Mater. Inter.* **11**, 17654 (2019).
- [47] N. Yu, P. Genevet, M. A. Kats, F. Aieta, J.-P. Tetienne, F. Capasso, and Z. Gaburro, Light Propagation with Phase Discontinuities: Generalized Laws of Reflection and Refraction, *Science* **334**, 333 (2011).
- [48] J. Mulkers, B. Waeyenberge, and M. V. Milosevic, Tunable Snell's law for spin waves in heterochiral magnetic films, *Phys. Rev. B* **97**, 104422 (2018).
- [49] J. F. Cochran and B. Heinrich, Boundary conditions for exchange-coupled magnetic slabs, *Phys. Rev. B* **45**, 13096 (1992).
- [50] V. V. Kruglyak, O. Y. Gorobets, Y. I. Gorobets, and A. N. Kuchko, Magnetization boundary conditions at a ferromagnetic interface of finite thickness, *J. Phys. Condens. Matter* **26**, 406001 (2014).
- [51] E. Hecht, *Optics* (Pearson Education Limited, Essex, 2017).
- [52] K. Tang, C. Qiu, J. Lu, M. Ke, and Z. Liu, Focusing and directional beaming effects of airborne sound through a planar lens with zigzag slits, *J. Appl. Phys.* **117**, 024503 (2015).
- [53] N. Yu and F. Capasso, Flat optics with designer metasurfaces, *Nat. Mat.* **13**, 139 (2014).
- [54] M. Jang, Y. Horie, A. Shibukawa, J. Brake, Y. Liu, S. M. Kamali, A. Arbabi, H. Ruan, A. Faraon, and C. Yang, Wavefront shaping with disorder-engineered metasurfaces, *Nat. Photonics* **12**, 84 (2018).
- [55] A. Conca, J. Greser, T. Sebastian, S. Klingler, B. Obry, B. Leven, and B. Hillebrands, Low spin-wave damping in amorphous $\text{Co}_{40}\text{Fe}_{40}\text{B}_{20}$ thin films, *J. Appl. Phys.* **113**, 213909 (2013).
- [56] P. Kuświk, H. Głowiński, E. Coy, J. Dubowik, and F. Stobiecki, Perpendicularly magnetized $\text{Co}_{20}\text{Fe}_{60}\text{B}_{20}$ layer sandwiched between Au with low Gilbert damping, *J. Phys. Condens. Matter* **29**, 435803 (2017).
- [57] A. V. Chumak, A. A. Serga, and B. Hillebrands, Magnonic crystals for data processing, *J. Phys. D: Appl. Phys.* **50**, 244001 (2017).
- [58] A. Maziewski, P. Mazalski, Z. Kurant, M. O. Liedke, J. McCord, J. Fassbender, J. Ferré, A. Mougín, A. Wawro, L. T. Baczewski, A. Rogalev, F. Wilhelm, and T. Gemming, Tailoring of magnetism in Pt/Co/Pt ultrathin films by ion irradiation, *Phys. Rev. B* **85**, 054427 (2012).
- [59] A. Wawro, Z. Kurant, M. Jakubowski, M. Tekielak, A. Pietruczik, R. Böttger, and A. Maziewski, Magnetic Properties of Coupled Co/Mo/Co Structures Tailored by Ion Irradiation, *Phys. Rev. Appl.* **9**, 014029 (2018).
- [60] S. Ikeda, K. Miura, H. Yamamoto, K. Mizunuma, H. D. Gan, M. Endo, S. Kanai, J. Hayakawa, F. Matsukura, and H. Ohno, A perpendicular-anisotropy CoFeB–MgO magnetic tunnel junction, *Nat. Mater.* **9**, 721 (2010).
- [61] V. B. Naik, H. Meng, J. X. Xiao, R. S. Liu, A. Kumar, K. Y. Zeng, P. Luo, and S. Yap, Effect of electric-field on the perpendicular magnetic anisotropy and strain properties in CoFeB/MgO magnetic tunnel junctions, *Appl. Phys. Lett.* **105**, 052403 (2014).
- [62] S. Miwa, M. Suzuki, M. Tsujikawa, T. Nozaki, T. Nakamura, M. Shirai, S. Yuasa, and Y. Suzuki, Perpendicular magnetic anisotropy and its electric-field-induced change at metal-dielectric interfaces, *J. Phys. D: Appl. Phys.* **52**, 063001 (2018).
- [63] B. Rana, S. Choudhury, K. Miura, H. Takahashi, A. Barman, and Y. Otani, Electric field control of spin waves in ultrathin CoFeB films, *Phys. Rev. B* **100**, 224412 (2019).
- [64] M. Vogel, A. V. Chumak, E. H. Waller, T. Langner, V. I. Vasyuchka, B. Hillebrands, and G. von Freymann, Optically reconfigurable magnetic materials, *Nat. Phys.* **11**, 487 (2015).
- [65] A. V. Sadovnikov, A. A. Grachev, S. E. Sheshukova, Y. P. Sharaevskii, A. A. Serdobintsev, D. M. Mitin, and S. A. Nikitov, Magnon Straintronics: Reconfigurable Spin-Wave Routing in Strain-Controlled Bilateral Magnetic Stripes, *Phys. Rev. Lett.* **120**, 257203 (2018).
- [66] J. Stigloher, M. Decker, H. S. Körner, K. Tanabe, T. Moriyama, T. Taniguchi, H. Hata, M. Madami, G. Gubbiotti, K. Kobayashi, T. Ono, and C. H. Back, Snell's Law for Spin Waves, *Phys. Rev. Lett.* **117**, 037204 (2016).
- [67] Z. Tian, C. Shen, J. Li, E. Reit, Y. Gu, H. Fu, S. A. Cummer, and T. J. Huang, Programmable Acoustic Metasurfaces, *Adv. Funct. Mater.* **29**, 1808489 (2019).
- [68] K. Y. Guslienko, S. O. Demokritov, B. Hillebrands, and A. N. Slavin, Effective dipolar boundary conditions for dynamic magnetization in thin magnetic stripes, *Phys. Rev. B* **66**, 132402 (2002).
- [69] F. Lisiecki, J. Rychły, P. Kuświk, H. Głowiński, J. W. Kłos, F. Groß, N. Träger, I. Bykova, M. Weigand, M. Zelent, E. J. Goering, G. Schütz, M. Krawczyk, F. Stobiecki, J. Dubowik, and J. Gräfe, Magnons in a Quasicrystal: Propagation, Extinction, and Localization of Spin Waves in Fibonacci Structures, *Phys. Rev. Appl.* **11**, 054061 (2019).
- [70] K. Vogt, H. Schultheiss, S. J. Hermsdoerfer, P. Pirro, A. A. Serga, and B. Hillebrands, All-optical detection of phase fronts of propagating spin waves in a $\text{Ni}_{81}\text{Fe}_{19}$ microstripe, *Appl. Phys. Lett.* **95**, 182508 (2009).
- [71] K. Baumgaertl, S. Watanabe, and D. Grundler, Phase control of spin waves based on a magnetic defect in a one-dimensional magnonic crystal, *Appl. Phys. Lett.* **112**, 142405 (2018).
- [72] A. Vansteenkiste, J. Leliaert, M. Dvornik, M. Helsen, F. Garcia-Sanchez, and B. V. Waeyenberge, The design and verification of MuMax3, *AIP Adv.* **4**, 107133 (2014).

Correction: An outdated manuscript file was inadvertently used for publication. The correct file has been processed, with changes to text in Sec. II A and to equations in Appendix A.